

# Extending the Dynamic Range of Electronics in a Time Projection Chamber

J. Estee<sup>a,b</sup>, W.G. Lynch<sup>a,b</sup>

<sup>a</sup>*Michigan State University, Dept. Physics and Astronomy*

<sup>b</sup>*National Superconducting Cyclotron Laboratory*

---

## Abstract

As Time Projection Chambers (TPCs) become widely utilized in low and intermediate nuclear physics experiments, it becomes important to extend the dynamic range to cover the large range in energy losses. In a recent set of experiments using the SAMURAI Pion-Reconstruction and Ion-Tracker (S $\pi$ RIT) TPC, it was important to simultaneously measure relativistic pions and heavy ions from the same collisions. A track which saturates the TPC electronics only does so for several pads near to the track while pads further away are not saturated. By performing a  $\chi^2$  fit using the pad response function on the unsaturated pads, we can recover the saturated pads charge. This resulted in an increase of the dynamic range by a factor of 2.

*Keywords:* `elsarticle.cls`, L<sup>A</sup>T<sub>E</sub>X, Elsevier, template

*2010 MSC:* 00-01, 99-00

---

## 1. Introduction

At low to intermediate heavy ion collision (HIC) energies, it may be necessary to measure particles that have a large variation in energy losses. Several techniques have been employed to address this issue in Time Projection Chambers (TPC). At the time of publication it is common for TPC electronics to have at best a signal to noise ratio of 1000:1. If the signal to noise ratio of at least 20:1 is required to measure minimum ionizing particles, (m.i.p.), around  $\beta\gamma = 0.4$  this means the maximum range we could expect would be 50x greater than m.i.p.

In heavy ion collisions (HIC) of 300 AMeV beam energies the range of particle  
 10 velocities ranges from m.i.p. to  $0.1\beta\gamma$ . These velocities cover about 40x the  
 $dE/dx$  of m.i.p. The energy loss scales like  $z^2$  for larger charged particles. Also,  
 if the track enters the TPC at an obtuse angle, the deposited charge on one pad  
 could be higher by a factor of about 4x. It becomes clear the large dynamic  
 range that must be covered in such intermediate HIC experiments. A couple  
 15 of TPC's such as the EOS TPC [?] or the AT-TPC were able to circumvent  
 the measuring of large energy deposits by lowering the gain in certain regions  
 either by lowering the voltage on the anode wires or electronics gain settings.  
 Of course the  $dE/dx$  resolution and accuracy of the momentum determination  
 goes down for light particles as only a subset of the whole TPC can be used.  
 20 Also there may be no  $dE/dx$  measurement for particles that avoid these regions.  
 Here we illustrate how to expand the dynamic range without these drawbacks  
 within the context of a standard multi-wire TPC.

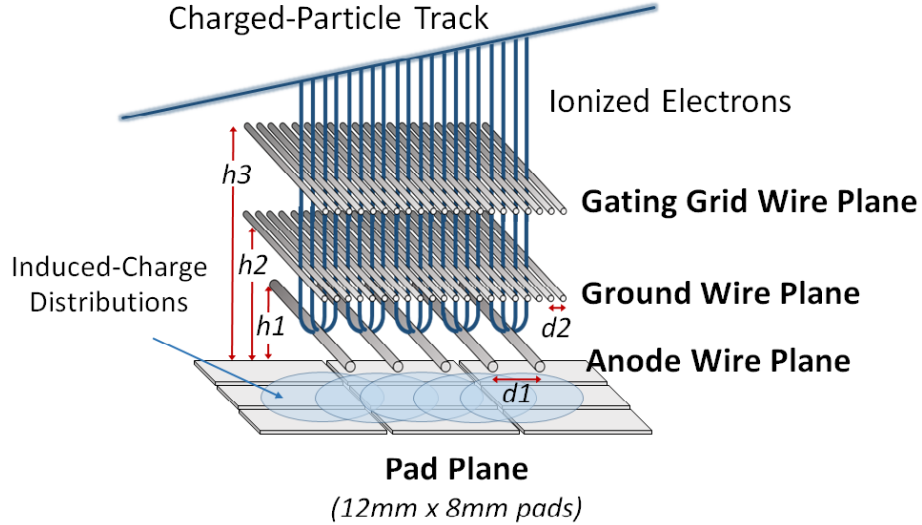


Figure 1: Cartoon graphic showing the 3 wire planes and a section of the pad plane.  $h3 = 14$  mm,  $h2 = 8$  mm,  $h1 = 4$  mm,  $d2 = 1$  mm,  $d1 = 4$  mm. The actual orientation is inverted from this picture but for ease of displaying this orientation fits best.

### 1.1 TPC Overview.

*Wire planes.* As seen in figure 1 the S $\pi$ RIT TPC consists of three wire grids  
 25 above the two dimensional array of charge sensitive readout pads, the pad plane.  
 The first two wire grids operate as a gate and a shielding, or ground grid, with  
 1 mm spacing and they are not important for the discussion of this paper. The  
 wire grid closest to the pad plane is the high voltage anode wire grid consisting  
 of 20  $\mu$ m wires spaced at 4 mm apart and set at a height of 4 mm from the  
 30 pad plane. In the near vicinity of these wires the avalanche of the preliminary  
 electrons occurs. The electrons deposited from tracks in the detector gas are  
 multiplied on the order of 2000 times and the slow moving ions induce a signal  
 on the read out pads below. The resulting distribution on the pad plane is fixed  
 by the geometry of the anode wire grid and its distance from the pad plane. The  
 35 anode wire planes were sectioned off into 14 independent sections. 12 sections of  
 the anode wire plane was held at 1460 V. This setting was optimized to ensure  
 the small signal of pions would at least have a signal to noise ratio of 20:1.  
 Two of the sections were held to 1214 V. The reduction in voltage resulted in a  
 reduction of about 10x gain compared to the higher anode wire sections. These  
 40 two sections of lower gain allow validation of the method that will be described.

*Pad plane.* The S $\pi$ RIT TPC pad plane consists of a 2-dimensional plane of  
 charge sensitive pads. Each pad is rectangular in shape with a dimension of .8  
 cm x 1.2 cm. It is laid out on a grid measuring 112 by 108 pads with a total  
 area of 134 cm x 86 cm. For convenience we have chosen the +x axis to point  
 45 to the right of beam, the -y axis as the direction pointing down into the drift  
 volume, and the +z axis along the incoming beam. The avalanche wires run  
 perpendicular to the beam axis along the x axis as seen in the figure 1.

*Generic Electronics for TPCs.* Signals from the pads in the S $\pi$ RIT TPC are  
 amplified and digitized by the newly developed Generic Electronics for TPCs  
 50 (GET) [? ]. Short cables transmit the signals from the pads to the inputs of  
 the AGET chips. Each AGET chip can service 64 pads and contains a Preamp  
 (PA), and a Switched Capacitor Array (SCA) with a maximum of 512 time  
 buckets sampling at 1 to 100 MHz. Four AGET chips are mounted on one

AsAd (Asic and Adc) motherboard. The gain of each AGET can be configured  
 55 as 0.12, 0.24, 1.0, or 10 pC over the whole dynamic range. Also the peaking  
 times of the shaping amplifiers can be set to 69, 117, 232, 501, 720, or 1014 ns.  
 The 12 bit ADC's on the AsAd boards deliver an effective 10.5 bit resolution.  
 For the first series of experiments the gain was set to the highest setting, 0.12  
 pC, and the peaking time was set to 117 ns. At such a high gain, the pion  
 60 signal was able to fully be measured. To put this gain setting into perspective,  
 the minimum velocity that would cause saturated pads was  $\beta\gamma \approx 0.2$  for  $z=1$   
 particles,  $\beta\gamma \approx 0.6$  for  $z=2$  particles, and  $z \geq 3$  particles were always saturating.

## 2. Pad Response Function

*Experimental PRF.* The fractional charge seen by each pad is referred to as  
 65 the Pad Response Function (PRF). Some simple wire plane geometries have  
 analytical expressions for the PRF which are well studied and may be looked  
 up using a Gatti distribution [? ]. When analytical PRFs do not exist, an  
 effective PRF may be calculated from experimental data. We postulate that  
 the PRF is only a function of the total charge deposited on the wire  $Q$  and the  
 70 displacement  $\lambda$ .

$$PRF(\lambda_i) = \frac{q_i(\lambda_i)}{Q}$$

$$\text{where } Q = \sum_i q_i \tag{1}$$

$$\text{and } \lambda_i = x_i - \bar{x}$$

When calculating the effective PRF from experiment, we selected data that  
 is not saturated, as this will only distort the shape of the PRF. Since the beam  
 comes in along the  $z$  direction, the  $x$  direction gives the best momentum reso-  
 lution and was the natural choice for clustering and calculating the PRF.

75 The PRF is given in equation 1 where  $i$  is the index over the pads and  $Q$   
 is the total charge within the layer. In figure 2, the estimate for the avalanche  
 position along the wire is given by the weighted mean position  $\bar{x}$ . Also seen is

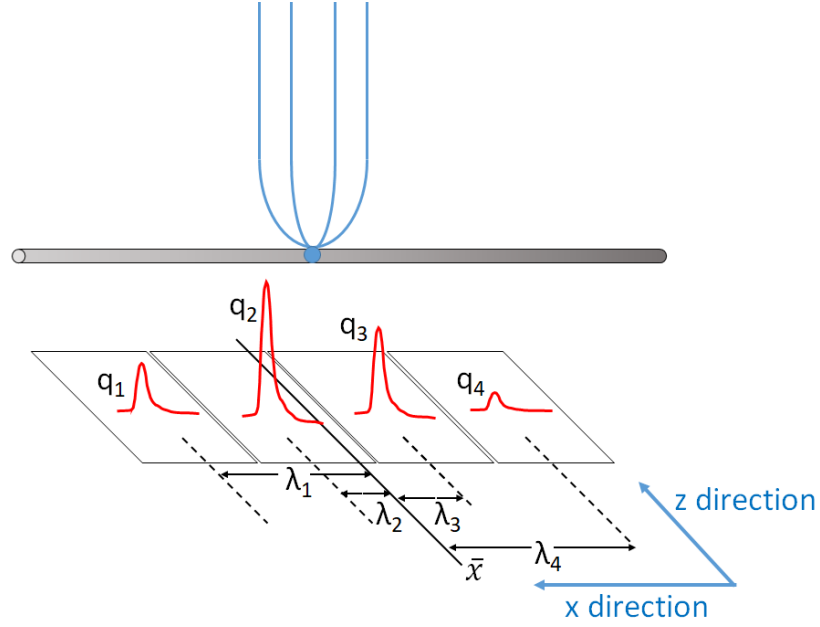


Figure 2: Cartoon graphic of avalanche event on an anode wire over one layer of pads. The estimate of the position of the avalanche is given by  $\bar{x}$  the weighted mean. The position from the center to each pad to the  $\bar{x}$  position is given as  $\lambda_i$ .

$\lambda_i$ , defined as the difference, in position, of the center of the  $i^{th}$  pad,  $x_i$ , to the mean position  $\bar{x}$ .

80 Calculating the PRF in the way described above, the resulting experimental PRF for the S $\pi$ RIT TPC is seen in figure ?? . The PRF obtained from averaging many events gives rise to a well behaved function. It is this function we will be using to fit the data to extend the saturated pads.

*Method of Desaturation.* Figure 4 shows a typical situation of saturated signals.  
 85 This will be used as an example to explain the method of extrapolating the saturated pads, referred to in this paper as desaturation. When an avalanche causes large induced signal, the pads directly underneath collect the largest charge and typically would be saturated. These are represented as  $q_{1'}$  and  $q_{2'}$  in the figure 4. The pads further away would experience smaller, non-saturated  
 90 signals.

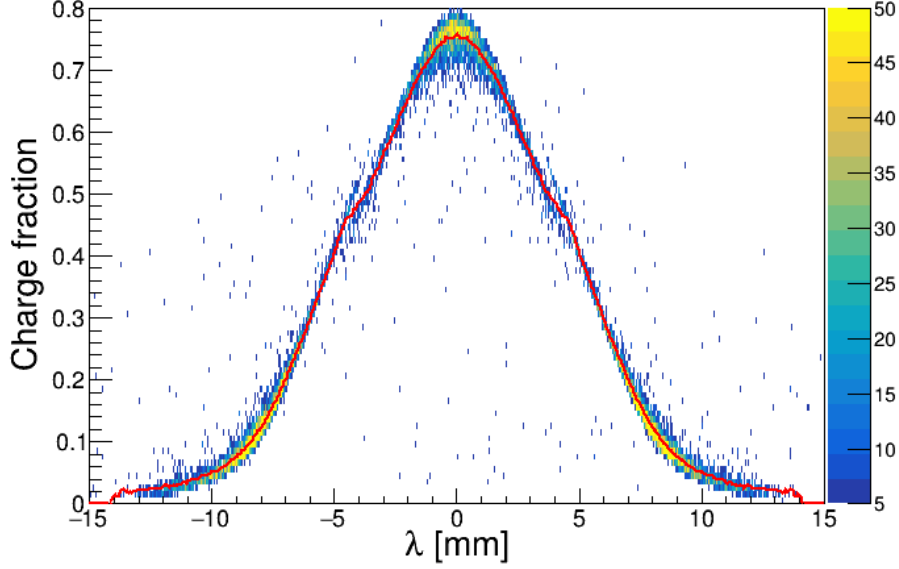


Figure 3: Experimental pad response function. Constructed from total number of pads  $\geq 3$ .

Since all the pad's charges must satisfy the PRF distribution described in figure 3, then using these small non-saturated tails we perform a  $\chi^2$  fit to find the unknown charge on the saturated pads.

### 3. Experimental data

Two sets of data will be discussed in this paper. The first set was a tuned cocktail beam consisting of (p,d,t, $^3\text{He}$ , $^4\text{He}$ , $^6\text{Li}$ , $^7\text{Li}$ ) light charged particles which was injected into the TPC for calibration purposes. The cocktail beam was tuned to two different  $\beta\rho$  settings and the momentum resolution was approximately 1% as determined by the slits of the BigRIPS fragment separator of the Radioactive Isotope Beam Factory (RIBF) facility in RIKEN. A thick 21mm thick aluminum target was inserted for part of the lower  $\beta\rho$  setting, further reducing the energy of the beam for a third calibration point.

In a typical cocktail event one particle enters the TPC volume at a time and mostly parallel to the pad plane. Thus, the cocktail beam data represents

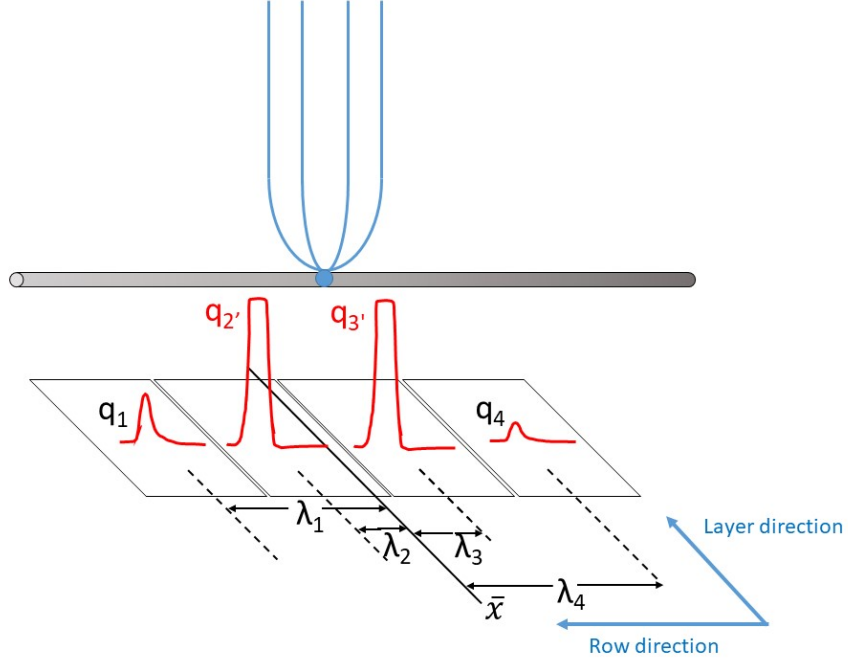


Figure 4:

105 an ideal case for the momentum and  $dE/dx$  determination as it does not suffer from inefficiencies related to high multiplicity events we see in the collision experimental data.

Shown in figure 5 is the typical pad plane response for a central nuclear collision of the system  $^{132}\text{Sn} + ^{124}\text{Sn}$ . During the experiment the voltages of two anode sections (as indicated by red arrows in figure 5) were turned down  
 110 from 1460 V to 1214 V. Since the anode voltages are dropped, the gain of these sections is also reduced by a factor of about 10.

#### 4. Results

*Low gain vs corrected high gain.* As mentioned above, two anode sections, covering 12 layers of pads in total, had their gain lowered by approximately a factor  
 115 of 10. The signals in this lowered gain region have effectively 10x the dynamic

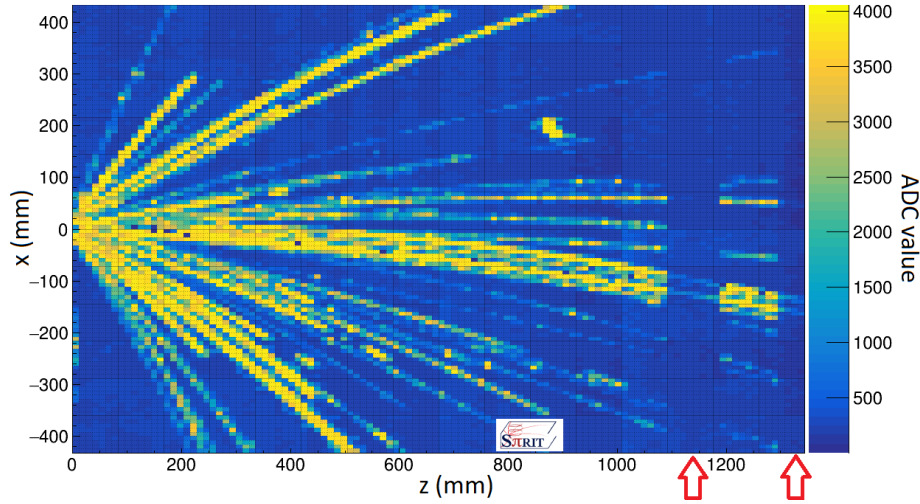


Figure 5: Pad plane projection for a collision event in the TPC. Highlighted by red arrows are two regions of anode wires which had a reduced voltage of 1214 V. The voltage of the rest of the TPC anode wires are 1460 V. The reduction in voltage reduces the gain by a factor of  $\approx 10$ .

range as compared with the high gain regions. That is to say when a track would saturate pads in the high gain region, the signal in this low gain region is still preserved and can be measured. By comparing the  $\frac{dE}{dx}$  values of the high gain sections with the low gain section we can determine whether the desaturation correction described above is successful.

It is clear from figure 6 the effect of saturation has on the high gain channels. The data starts to saturate and deviates from the  $y=x$  line around about 400 ADC/mm in the high gain channels and eventually plateaus. After applying the desaturation correction the correlation between the high gain and low gain sections is significantly restored as seen in figure 7. Judging by the corrected correlation plot we can believe the correction to at least about 900 ADC/mm. It seems the 1:1 correlation is mostly restored and the increase in dynamic range in the high gain pads is about a factor of 2x.

*Particle Identification (PID).* Comparing the low to high gain sections provides a direct comparison for determining the success of the extrapolation. The true



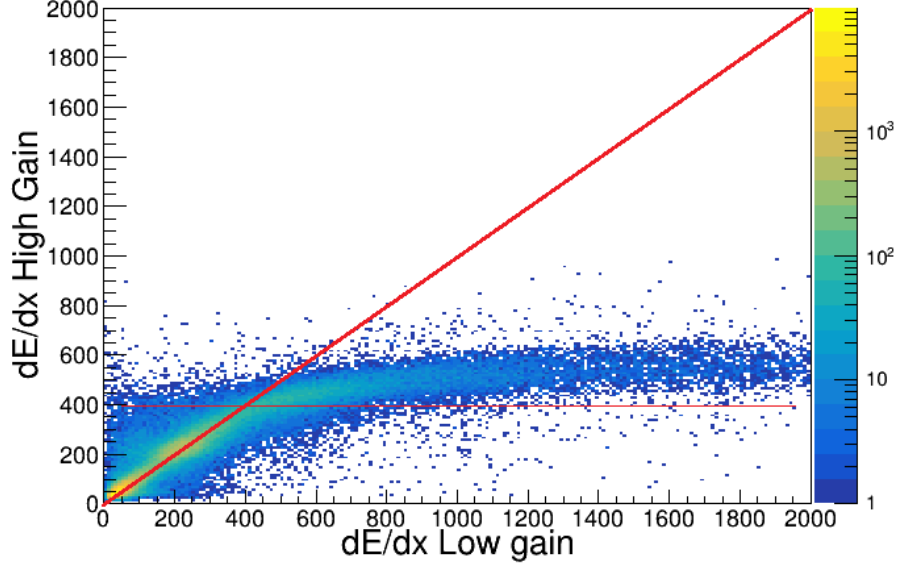


Figure 6: The uncorrected high gain dE/dx vs low gain dE/dx collision data.

goal of any correction would be to improve the PID.

Looking firstly at the ideal case of the cocktail beam in figures 8 and ?? we note the very clean pronounced PID lines of several particle species. Once  
 135 can clearly see the three  $B\rho$  settings of the fragment separator leading to three ovals around 1700 and two near 900 [MeV/c/Z]. The tails of the PID lines leading away from these three ovals are resulting from the particle losing its initial energy by passing through the walls and other materials outside the main detector volume. Looking at the uncorrected data in figure 8 we can see the  
 140 effects of saturation. The experimental PID deviates from the theoretical values given by the red curves. It seems the dE/dx values plateau starting around 400 ADC/mm as we also saw in figure 6. After applying the desaturation method we see a stark difference in figures ?? and 11. Most notable is the difference between He and Li particle species which suffer the most from saturation. Perhaps the  
 145 more subtle improvement of the lighter particles, (p,d,t), can also be seen in the PID values at lower momentum.

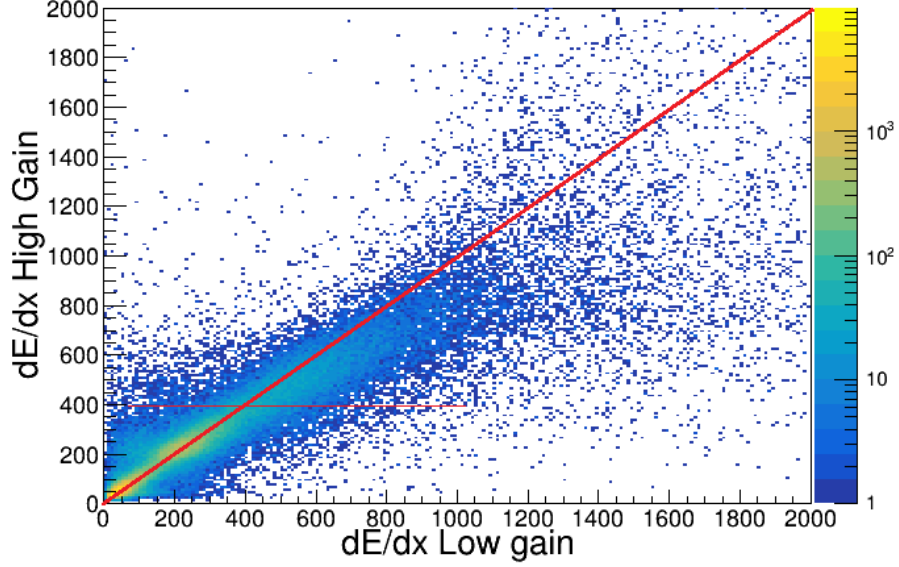


Figure 7: The corrected high gain  $dE/dx$  vs low gain  $dE/dx$  for ??? events of collision data.

## 5. Conclusion

We have shown that one can easily construct the Pad Response Function from unsaturated experimental data. Using this function and applying a simple  $\chi^2$  fit to the unsaturated tails of data, one can recover the saturated pad charge in the middle of the distribution because the true PRF is fixed by the anode wire geometry. We also demonstrated the success of this method by a direct comparison of  $dE/dx$  obtained in the high gain sections, to the true unsaturated  $dE/dx$  value obtained in the low gain sections which give the true unsaturated  $dE/dx$  value. This simple method gives significant improvement to the PID of particle and improves the dynamic range by a factor of at least 2.

## References

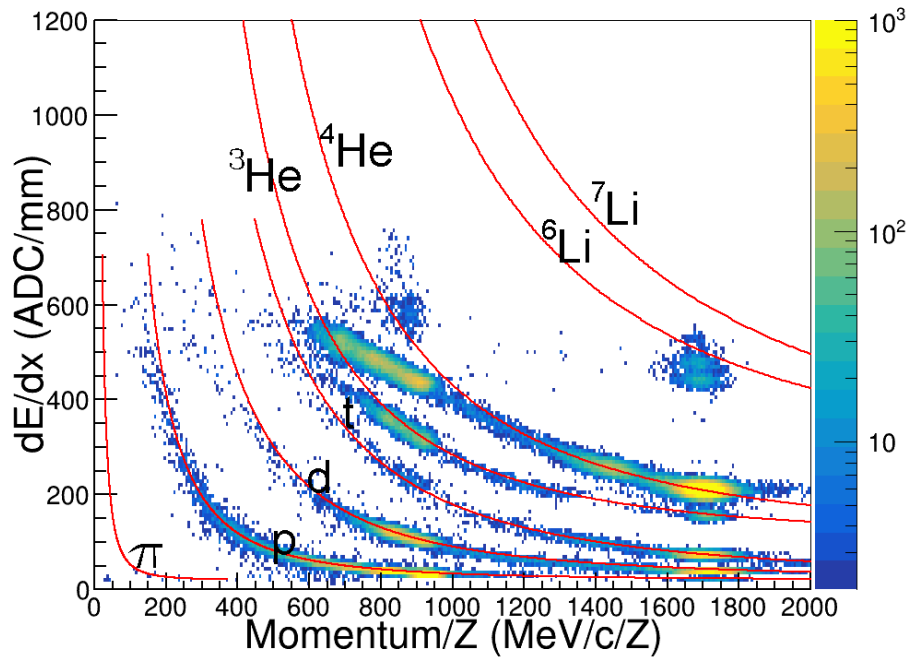


Figure 8: Uncorrected cocktail data.

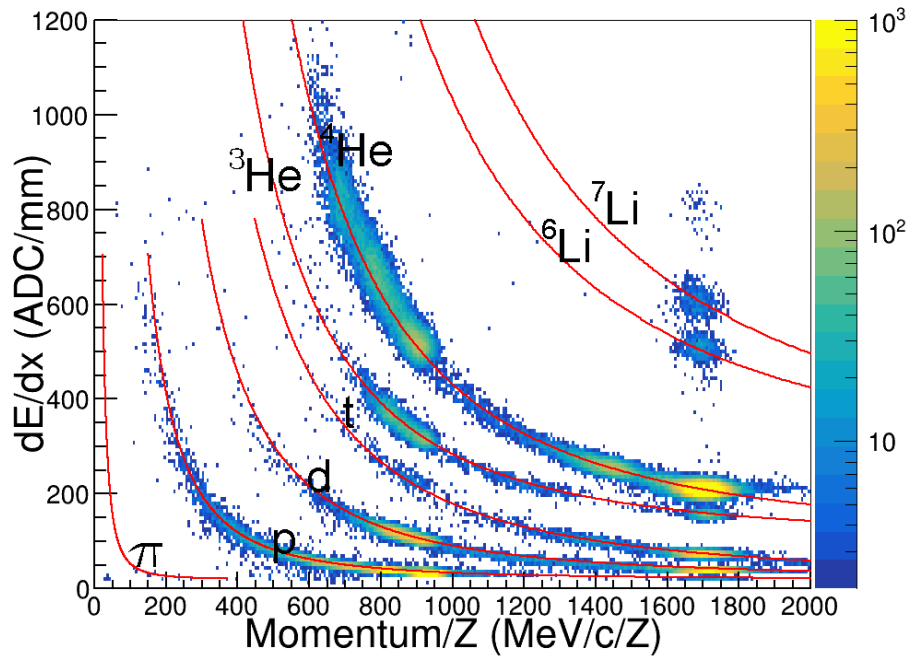


Figure 9: Corrected (desaturated) cocktail data.

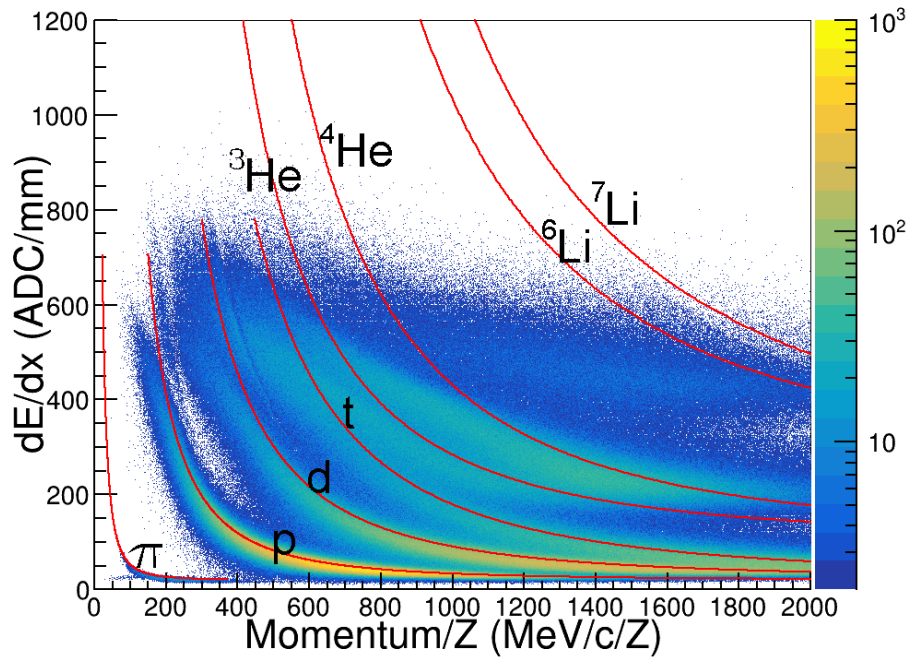


Figure 10: Uncorrected collision data.

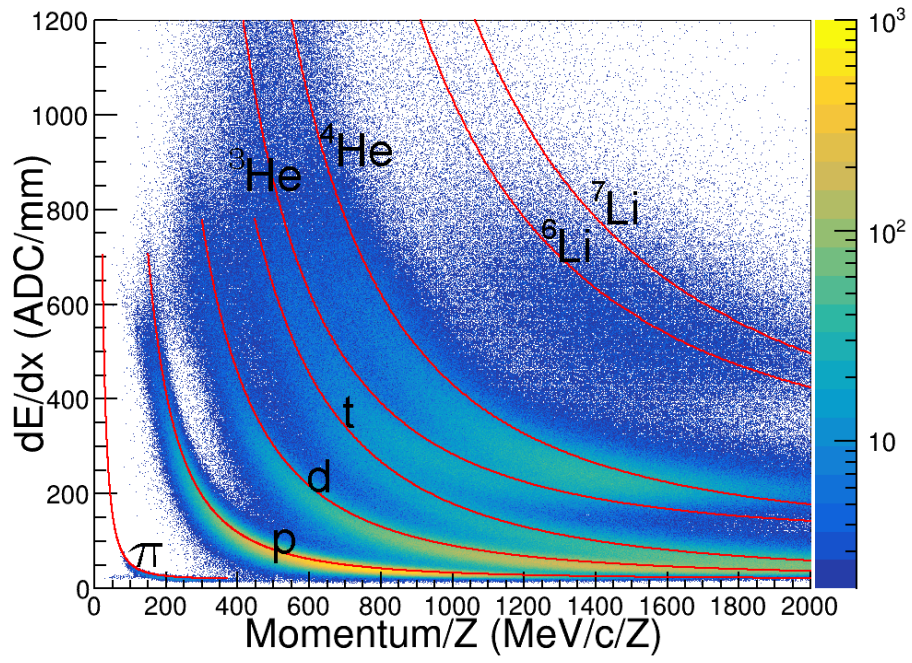


Figure 11: Corrected (desaturated) collision data.